

# Data-Driven, Physics-Based Feature Extraction from Fluid Flow Fields using Convolutional Neural Networks

Carlos Michelén Ströfer<sup>1,\*</sup>, Jin-Long Wu<sup>1</sup>, Heng Xiao<sup>1</sup> and Eric Paterson<sup>1</sup>

<sup>1</sup> Kevin T. Crofton Department of Aerospace and Ocean Engineering, Virginia Polytechnic Institute and State University, Blacksburg, VA, USA.

Received 5 February 2018; Accepted (in revised version) 31 May 2018

---

**Abstract.** Feature identification is an important task in many fluid dynamics applications and diverse methods have been developed for this purpose. These methods are based on a physical understanding of the underlying behavior of the flow in the vicinity of the feature. Particularly, they require the definition of suitable criteria (i.e. point-based or neighborhood-based derived properties) and proper selection of thresholds. However, these methods rely on creative visualization of physical idiosyncrasies of specific features and flow regimes, making them non-universal and requiring significant effort to develop. Here we present a physics-based, data-driven method capable of identifying any flow feature it is trained to. We use convolutional neural networks, a machine learning approach developed for image recognition, and adapt it to the problem of identifying flow features. This provides a general method and removes the large burden placed on identifying new features. The method was tested using mean flow fields from numerical simulations, where the recirculation region and boundary layer were identified in several two-dimensional flows through a convergent-divergent channel, and the horseshoe vortex was identified in three-dimensional flow over a wing-body junction.

**AMS subject classifications:** 76G25, 76M99

**Key words:** Machine learning, feature identification, fluid dynamics, convolutional neural network.

---

## 1 Introduction

Feature detection is an important component of data post-processing in fluid dynamics experiments and simulations, and plays an important role in our physical understanding

---

\*Corresponding author. *Email addresses:* cmich@vt.edu (C. Michelén Ströfer), jinlong@vt.edu (J.-L. Wu), hengxiao@vt.edu (H. Xiao), egp@vt.edu (E. Paterson)

of flow phenomena and fluid-structure interactions. In this study we use convolutional neural networks, a machine-learning approach developed for image recognition, to automatically detect features of interest in fluid flow fields. As with traditional methods, feature detection is done by identification of patterns within the relevant physics-based scalar fields of the flow. Unlike traditional methods, the specific patterns to use are not explicitly specified, but inferred from a set of human-labeled training examples.

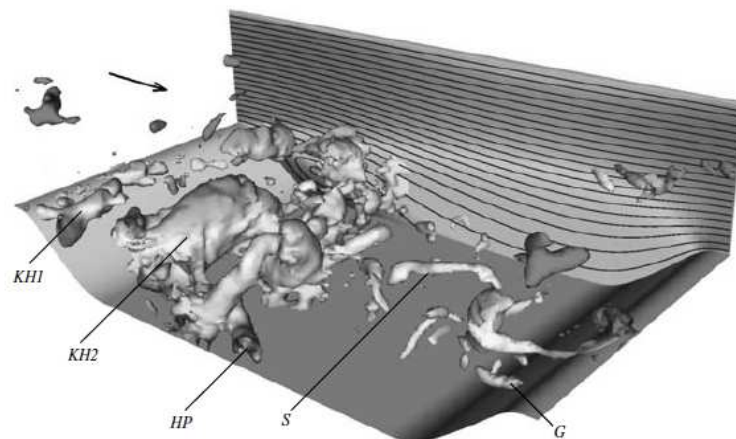
## 1.1 Feature detection in fluid flow fields

A flow feature is a physically meaningful structure within the flow that is of interest for the application at hand. Examples include recirculation regions, shed vortices, boundary layers, and shock waves. Applications of flow feature extraction include fundamental physical understanding of flow dynamics (e.g. relation between coherent structures and turbulence dynamics [1, 2]), engineering design (e.g. reduction of shock wave drag [3]), on-line steering of large simulations (e.g. feature-based adaptive mesh [4, 5]), among others. Despite the important role flow features play in so many applications, the task of accurately identifying these features remains a laborious one.

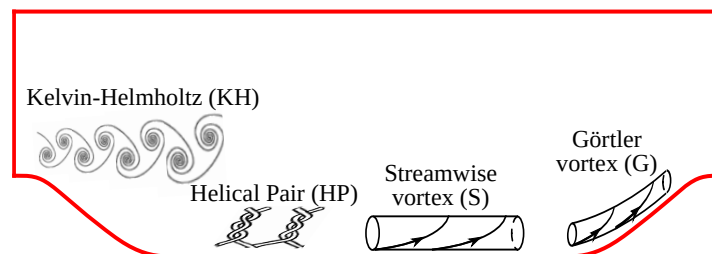
Post et al. [6] describe the general *feature extraction pipeline* as consisting of four steps: selection, clustering, attribute calculation, and iconic mapping. *Selection* consists of identifying all points that are part of the feature of interest, and the output of this step is a binary map. In the *clustering* step these points are divided into discrete instances of the feature of interest. For instance, the input to the clustering step might be a binary map of points that belong to vortices, and the output are groupings of these points into coherent regions, e.g. distinct vortices. The last two steps, *attribute calculation* and *iconic mapping*, consist of calculating properties of each coherent region (e.g. volume, length, centroid) and fitting a parametrized icon (e.g. ellipsoid). This has the effect of reducing the dimensionality of the problem, allowing the description of the evolution of features with only a few parameters. In this paper we focus on the first two steps, *selection* and *clustering*, and only imply these steps when referring to *feature extraction* or *identification*.

Many methods exist for identifying features based on an understanding of the underlying physics of the phenomena. As an example, methods for identifying vortices include identification based on local field values (e.g. vorticity, helicity,  $Q$ -criterion), as well as methods based on global flow properties (e.g. curvature center, looping streamlines) [6]. The disadvantages with these methods are that they are specific to the feature in question, limited to certain types of flows (e.g. external flows, turbo-machinery) [6], and rely on creative visualization of the physical phenomena at hand. This has led to many disjoint methods particularly suited for very specific problems, and places a large burden on developing methods for identifying new features.

As a specific example of the need for improved flow feature extraction we consider the problem of turbulence. Turbulent flows contain temporally-coherent structures (flow features) at various scales. These coherent structures are known to play an important role in mass, momentum, and energy transport [1, 2] and subsequently have an effect on



(a) Coherent structures from large eddy simulation, reproduced with permission from Fröhlich et al. [7]



(b) Schematic of coherent structures

Figure 1: Distinct vortex structures in the flow over periodic hills as identified by using isosurfaces of pressure fluctuations from large eddy simulation data (a) reproduced with permission from Fröhlich et al. [7], and a schematic representation of such coherent structures (b). The types of vortices shown are: Kelvin-Helmholtz vortices (KH), helical pairs of span-wise vortices (HP), streamwise vortices (S), and Görtler vortices (G).

overall flow dynamics. Despite this fact, existing turbulence models used for predicting flow separation rely on time-averaged quantities and ignore the presence of coherent structures. For instance, Fröhlich et al. [7] found that the “splating” of large-scale eddies originating from the shear layer results in a high-level of spanwise velocity fluctuations in the post-reattachment, which existing turbulence models fail to capture. Fig. 1 shows an example of these turbulent coherent structures in a flow over periodic hills, showing the large number of distinct types of features and scales present in turbulent flows. For instance, Fig. 1 shows Kelvin-Helmholtz vortices in the leeward side of the hill and a Görtler vortex in the windward side.

Fundamental understanding of turbulence and development of better predictive models requires establishing a link between organized fluid motion and turbulence statistics. The failure to establish such a link is largely attributed to the lack of reliable data and the lack of effective feature identification techniques for extracting physically significant

coherent structures. Effective feature identification would require the ability to automatically search through large time-resolved datasets, search for structures at many scales, and differentiate between similar features (e.g. different types of vortical structures as shown in Fig. 1). Existing methods, such as visualization of contours and isosurfaces of flow field variables (e.g.  $u'$ ,  $p'$ ,  $\lambda_2$ , and  $Q$ -criterion), require careful choice of criterion and threshold which can be flow and structure dependent. This process requires iterative visualization and relies on expert prior knowledge of the specific form of the structure, making it unpractical for large number of time-resolved simulations. Moreover, previous studies [7,8] reported that the identification with existing physics-based approaches turned out to be even more difficult at high Reynolds number flows, where large-scale structures are likely to be overwhelmed by small-scale eddies.

In this paper we provide a universal method for flow feature identification that could replace or supplement the myriad of existing disjoint methods and remove the large burden placed on developing methods for identifying new features. The method is based on convolutional neural networks, a machine learning algorithm used in image recognition, and learns to find structure within the data solely from the examples it is trained with. The approach is fundamentally different to existing methods in that it is data-driven rather than based on explicitly defined physics. This is still physics-based in that the features are identified by searching for relevant structures within scalar fields of physical quantities, but these relevant structures are inferred from the data rather than explicitly defined. This has the advantage of being a general approach, and allowing for the identification of new features for which explicitly defined physics approaches do not exist. The method also has the potential of being more discerning between similar features than existing methods, provided sufficient training data. The use of this type of machine learning methods has gained popularity in science and engineering applications in recent years with promising results (e.g. [9]). While flow feature extraction from time-resolved flow fields (e.g. coherent structures in Fig. 1) is an important future application, in this initial study we extract flow features from mean flow fields.

## 1.2 Machine learning for object detection in images

Machine learning is a class of algorithms that makes decisions based on learned parameters from data, rather than from explicit instructions. The machine learning algorithms used in this paper were adapted from image recognition and object detection, and an analogy is made between these tasks and flow feature detection. *Image recognition* consists of classifying an image of a single object as belonging to some class (e.g. car, person). *Object detection* consists of finding and classifying all objects within an image that contains more than just a single object. Fabricated examples of image recognition and object detection are shown in Fig. 2. Both of these tasks can be achieved using different machine learning algorithms. In this paper we consider the object detection R-CNN method developed by Girshick et al. [10,11] and adapt it to the problem of flow feature extraction. The R-CNN method consists of two main steps, a region proposal step that identifies sub-

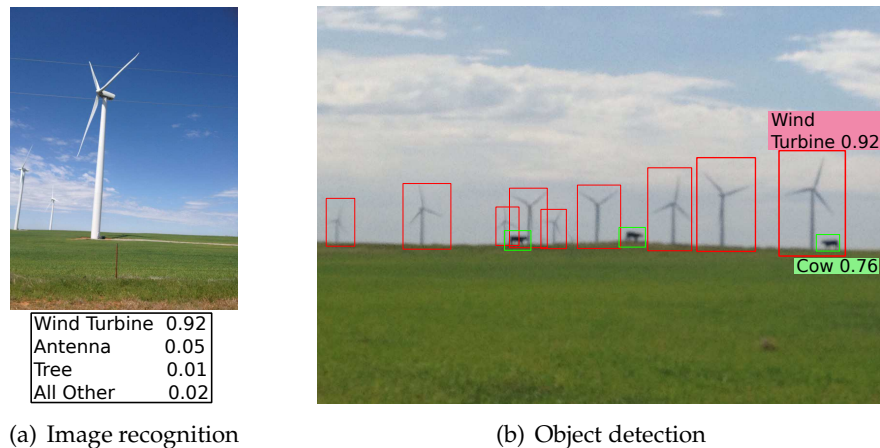


Figure 2: Fabricated examples of image recognition (a) and object detection (b) tasks in images. The number indicates the probability of the region or image being an instance of the specified class. The labels for only two of the “detected” objects in (b) are shown.

images containing objects of interest, and an image recognition step using convolutional neural networks (CNN) that classifies those sub-images into appropriate classes.

Neural networks are a class of machine learning algorithms that are universal estimators. That is they can be used to estimate any function to any desired accuracy by choice of complexity. Neural networks consist of sequential layers of variables, referred to as neurons, with the first and last layer corresponding to the inputs and outputs respectively. The number of neurons in the first and last layer are determined by the dimensions of the inputs and outputs, while the number of intermediate layers and the size of each are free hyper-parameters chosen to achieve a desired level of complexity. Specific non-linear mappings are defined between adjacent layers, hence an input can be propagated forward through the network resulting in an output. The parameters of these non-linear mappings are learned from a set of training data. The specific choice of layers and mappings is referred to as the network architecture. While neural networks are universal estimators, estimating an image classification function can require complex architectures with a large number of trainable parameters.

Convolutional neural networks (CNN) [12–14] are a class of neural networks that exploit known functional structures in the image classification problem in order to simplify the network architecture and speed up training. Specifically CNNs use convolutional layers which exploit translational invariance (e.g. whether a region of the image contains an object of interest does not depend on the location of the region relative to the whole image), greatly reducing the number of neurons. Informally a convolutional layer can be thought of as scanning the image searching for different local-features (e.g. horizontal lines, gradients), and creating a local-feature map for each. Convolution layers can be used sequentially, identifying increasingly more complex patterns with the largest scale patterns used for the final classification.

### 1.3 Machine learning for feature detection in fluid flow fields

The problem of flow feature detection is analogous to the problem of object detection in that flow features make a subset of the input and can be found anywhere within the flow. For this reason the authors believe the R-CNN method, and CNNs in general, are well suited for the task of flow feature extraction. However, adapting these algorithms to physical flows presents some unique challenges.

The first challenge is in representing the flow in a manner conducive to the application of these algorithms. An image is represented with three invariant (i.e. not dependent on choice of coordinates) RGB color values at each pixel. Similarly, we represent the flow by a suitable list of invariant physical properties at each of a number of discrete points. The second challenge is that while algorithms developed to use images require inputs with rectangular domains, the physical domain of fluid flows is generally not rectangular, containing boundaries of arbitrary shape as well as holes in the domain where solid objects exist. To circumvent this challenge, in this initial study flows were restricted to flows with singly-connected domains, and were mapped to rectangular domains. The last challenge is that while objects in images can be identified using rectangular bounding boxes of moderate aspect ratios that mostly contain only the object in question, not all flow features can be identified in this manner. To address this we distinguish between what we call *discrete features* such as shed vortices which can be encompassed by a bounding box and *continuous features* such as boundary layers which cannot. Continuous feature problems have no analog to image recognition and the approach taken was to provide a boolean field of points that belong to that feature, rather than a rectangular bounding box. This corresponds to performing the *selection* step, but not the *clustering* step in the *feature extraction pipeline* [6].

One final note on nomenclature: this paper combines concepts from different fields and there is a terminology conflict that must be addressed. In image recognition the goal is to detect objects within the image, and this is done by first identifying smaller scale patterns (e.g. horizontal lines, or sharp gradients) referred to as *features*. The conflict arises in that in fluid flows the 'objects' to be detected are also referred to as *features*. We will avoid ambiguity by referring to these as *local-features* and *flow features* respectively. The term *feature* is also commonly used to describe the point-based properties of the flow, but these will be referred to as input parameters.

## 2 Methodology

The methodology, which we will refer to as Fluid R-CNN, is adapted from the R-CNN method [10, 11] to work for fluid flow feature identification. The Fluid R-CNN can be divided into four steps. First, the flow is represented as a three-dimensional rectangular grid, with each point described by a list of invariant physical flow properties, analogous to the three RGB values used to describe pixels in images. Next, in the region proposal step, subsets of the flow are selected for classification. In the classification step, the pro-

posed regions are evaluated using a trained CNN and classified as being either an instance of the flow feature of interest or as background. Finally, in the selection step, the information from all the region evaluations is used to select and report the number and location of flow features.

## 2.1 Input array

The starting point of the method are fluid flow fields such as those obtained from either mean or time-resolved simulations or experimental data. In particular for the case studies presented here they are mean fields from Reynold-averaged Navier-Stokes (RANS) simulations. Following the procedures in Wang et al. [15] and Ling et al. [16], ten input parameters are used to characterize the flow at each cell. These parameters are non-dimensional, Galilean invariant, and based only on the flow properties at that point. The ten input parameters are summarized in Appendix A and include turbulence intensity, non-orthogonality of velocity and its gradient, and streamline curvature.

In these test cases we restrict our inputs to flows with a simply-connected domain and uniform mesh. The uniform mesh can be directly represented as a rectangular three-dimensional array, with each element corresponding to a mesh cell and having associated  $(x,y,z)$  coordinates, cell volume, and ten-dimensional input. This array representation of the flow fields is the input to the Fluid R-CNN method, and is referred to as the *input array*.

## 2.2 Region proposal

While many region proposal algorithms are being developed [10] that can efficiently produce proposals for objects in thousands of classes, a brute search approach was used. The brute search consists of searching the input array with a number of windows of different shapes, using specified stride length. All the resulting regions are considered possible flow features to be classified by the CNN. Brute search does not add significant computational cost in the test cases presented since only a single flow feature is being searched for (binary classification). The advantage of more sophisticated region proposal algorithms is more evident when a large number of classes are considered.

A consequence of scanning a rectangular representation of the flow is that since elements of the input array correspond to cells with different volumes, a scanning window of fixed dimensions (e.g.  $n \times m$  cells) will result in regions of vastly different physical shapes and dimensions. Fig. 3 shows a rectangular subregion of the input array, and its corresponding region in the physical domain. A second consideration is that the CNN only accepts rectangular inputs of a fixed size, while the region proposal selects regions of different sizes and aspect ratios. This second problem is shared with object detection in images, where region proposals might have different size and aspect ratios than the CNN input, and is solved by warping the image and using a CNN trained with warped images.

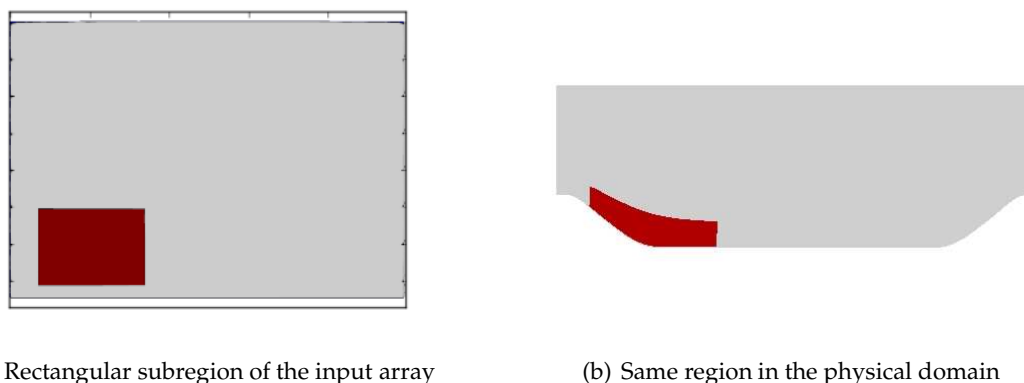


Figure 3: Example of a rectangular sub-region of the input array (a), and its corresponding region in the physical domain (b). This example corresponds to the human-labeled recirculation region for the 2D periodic hills flow.

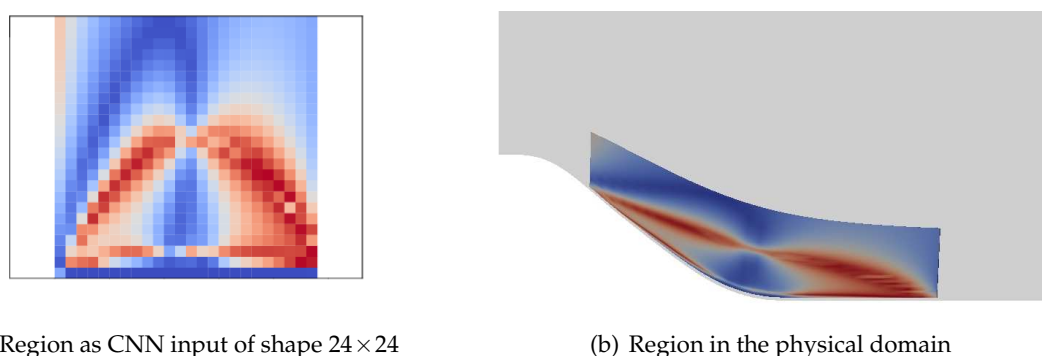


Figure 4: Mapping of a proposed region in the physical domain (b) to CNN input (a). The example region corresponds to the region shown in Fig. 3, and the input shown is the non-orthogonality of velocity and its gradient.

The goal is then to map each proposed region into a rectangular region of the specified size, with as little deformation as possible. This was done by first normalizing each element in  $[:,j,k]$  rows based on the cells'  $x$ -coordinates, each element in  $[i,:,k]$  rows based on the cells'  $y$ -coordinates, and each element in  $[i,j,:]$  rows based on the cells'  $z$ -coordinates. This, now rectangular, region is interpolated to a uniform grid with the required CNN input dimensions. The process is illustrated in Fig. 4.

### 2.3 Classification using CNN

Following the region proposal step, each proposed region must be classified. The classification step is done using a convolutional neural network, trained to differentiate between background regions and regions containing the feature of interest. The first step in cre-

ating a CNN is determining its architecture. The architecture must be flexible enough to make the classification task possible, while being simple enough to keep the number of training parameters and computational cost low. The second step is training the CNN, in which the optimal values for the trainable parameters are learned based on the training examples provided.

### 2.3.1 CNN architecture

The CNN architecture was designed with the goal of obtaining as simple a network as possible, while still being able to correctly identify the features of interest. All cases in this study use a similar CNN, with a single convolutional layer, a pooling layer, and an output layer consisting of 2 softmax neurons. A schematic of the CNN architecture used in this study is shown in Fig. 5. For clarity of illustration, Fig. 5 shows an input with only two physical dimensions rather than the full 3 dimensions actually used.

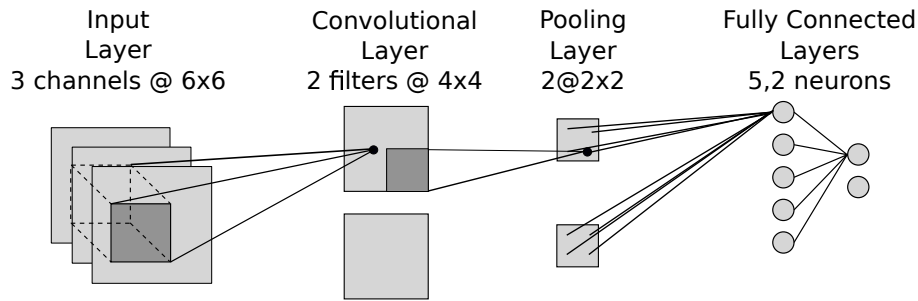


Figure 5: Example schematic of the CNN architecture with one convolutional layer with 2 feature maps and a pooling layer, followed by two dense layers, the first with 5 linear rectified neurons, and the output layer with 2 softmax neurons. For clarity of illustration, the input layer is shown as having two physical dimensions rather than all three. For each layer following the input layer, the schematic shows the input for a single value in that layer.

The input layer corresponds to a region in the flow domain, with each input point described by a ten-dimensional input vector (10 channels). This input layer is a tensor of size  $N_c \times N_x \times N_y \times N_z$ , where  $N_c$  is the number of channels and  $N_x, N_y, N_z$  are the number of points in each spatial dimension. The input layer is followed by a convolutional layer, which consists of  $N_f$  local-feature maps. Each map contains information of the presence of a specific local-feature (e.g. a sharp gradient, or a horizontal line) at different locations in the input. The map is created by sliding a window through the spatial dimensions of the input layer, outputting a single neuron activation value at each location considered. The sliding window over the inputs is called the *local receptive field* and has dimensions  $N_c \times N_{fx} \times N_{fy} \times N_{fz}$ . The neuron activation chosen is the rectified linear unit (ReLU), with activation given by

$$y = \max\left(0, \sum_{i=1}^{N_{rf}} (w_i x_i) + b\right), \quad (2.1)$$

where  $N_{rf}$  and  $x_i$  are the number of inputs and the individual elements in the local recep-

tive field respectively, and  $w_i$  and  $b$  are the *weights* and *bias* respectively. The weights and the bias are parameters that need to be determined through training. These weights and bias are the same for all spatial locations, i.e. when the local receptive field is moved to a different location in the input the weights and bias are unchanged. This enforces translational invariance, greatly reducing the number of trainable parameters. The example in Fig. 5 has a two-dimensional input of size  $6 \times 6$  with 3 channels ( $N_c = 3$ ,  $N_x = 6$ ,  $N_y = 6$ ). The input layer is followed by a convolutional layer with two filters, each with a local receptive field of shape  $3 \times 3 \times 3$  ( $N_c = 3$ ,  $N_{fx} = 3$ ,  $N_{fy} = 3$ ) and stride length of one in both directions, resulting in the local feature maps of size  $4 \times 4$ .

Immediately following the convolutional layer is a pooling layer, which has the role of condensing the information and reducing the size of the input. It does this by dividing the feature maps into windows of specified size (stride length is window dimensions) and summarizing each region with a single value. Max pooling was used for this purpose, where the output is the maximum value in the window. This results on information on whether the feature is found *anywhere* in that window. These could potentially be followed by more convolution-pooling layer pairs with the goal of identifying higher scale features from smaller scale features, but for simplicity only one convolutional layer was used. The example in Fig. 5 has a max pooling layer with input of size  $(2 \times 2)$ , which condenses each feature map (size  $4 \times 4$ ) to size  $2 \times 2$ .

Finally, the CNN has one or more layers of fully connected neurons, with the output layer being a *softmax* layer of size equal to the number of categories being considered. Each neuron in a softmax layer outputs a probability of the input belonging to that category, with the sum of all the outputs equal to one. The output of the softmax neuron is given by

$$y_i = \frac{e^{z_i}}{\sum_{j=1}^{N_{curr}} e^{z_j}}, \quad (2.2)$$

$$z_j = \sum_{k=1}^{N_{prev}} (w_{k,j} x_k) + b, \quad (2.3)$$

where  $N_{curr}$  and  $N_{prev}$  are the number of neurons in the current (softmax) and previous layers respectively, and  $x_k$  and  $w_{k,j}$  are the output and weight from the  $k^{\text{th}}$  neuron of the previous layer to the  $j^{\text{th}}$  neuron of the current layer. In this study ReLU neurons are used for all intermediate layers and two softmax neurons are used as the final layer, classifying the input as belonging to the feature of interest or to the background. For all cases the weights were initialized by sampling a normal distribution with mean zero and standard deviation 0.1, and all biases were initialized to zero.

### 2.3.2 CNN training

The first step in training the CNN is creating examples of regions that are instances of the flow feature of interest and examples of regions that belong to the background. For

discrete features the training inputs are the entirety of the flow field with the instances of the flow features of interest labeled. Labeling is done by identifying a bounding rectangle that completely encloses the flow feature of interest. Each labeled region can provide many training examples by shifting the bounding box and considering partial overlap [10]. Using different window sizes, the training case is scanned to create potential training examples. For each potential example, the maximum intersection over union (IoU) with a labeled region is calculated based on cell volume. The IoU for two regions  $A$  and  $B$  is given by

$$IoU(A,B) = \frac{A \cap B}{A \cup B}, \quad (2.4)$$

where  $A \cap B$  and  $A \cup B$  denote the volume of their intersection and union respectively. Regions with IoU above a certain threshold (e.g. 50%) are considered examples of the flow feature. Those below the threshold are considered background. Furthermore those in the background that have an IoU larger than some second threshold (e.g. 25%) are considered difficult examples [10] of the background. These regions are then down-sampled to the desired number of training cases, ensuring sufficient examples of each category are retained.

The CNN is then trained, with the data prepared as above. Training consists of optimizing the CNN parameters, i.e. the biases associated with each neuron and the weights associated with each connection. The training is done using stochastic gradient descent [12] and back-propagation [12, 17], with a categorical cross-entropy cost function. No dropout or regularization was used. Using gradient descent, each parameter  $a_i$  (weights and biases) is updated as

$$a_i^{(n+1)} = a_i^{(n)} - \gamma \nabla C(a_i), \quad (2.5)$$

where the superscript indicates the update step, the learning rate  $\gamma$  is a hyper-parameter, and  $C$  is the cost function which depends on all the parameters  $a_i$  and all the training examples. The categorical cross-entropy cost function is given by

$$C = -\frac{1}{N_t} \sum_{j=1}^{N_t} \sum_{i=1}^{N_{cat}} t_{i,j} \ln(p_{i,j}), \quad (2.6)$$

where  $t_{i,j}$  and  $p_{i,j}$  are the true and predicted values of the  $i^{\text{th}}$  output neuron for the  $j^{\text{th}}$  training example,  $N_{cat}$  is the number of categories (i.e. number of neurons in last layer), and  $N_t$  is the number of training examples. For a given training case ( $j$ ) one  $t_{i,j}$  has a value of one and all others have a value of zero. Stochastic gradient descent refers to approximating the gradient of  $C$  using only a random subset (mini-batch) of the training data at each update step. Back-propagation is a method to calculate the gradients of  $C$  with respect to each weight and bias by applying the chain rule to iteratively obtain the gradients at each layer, starting from the output layer.

At each training iteration a mini-batch is created with a random selection of a specified number of training examples. Each mini-batch is forced to contain a certain proportion of each type of examples (e.g. 50% easy background examples, 25% difficult background examples, and 25% flow feature examples). This is to ensure the training sees enough examples of the flow feature and difficult background examples. The training goes on until an acceptable convergence is seen in the cost function.

The training for continuous features is similar except that section cuts of the original flow are used as the training cases, rather than the entire flow domain. The flow feature of interest is only identified and labeled in these section cuts. This procedure was chosen because for continuous features a single bounding box mostly containing the flow feature is not possible in the whole domain, but is possible in section cuts of the domain.

## 2.4 Selection

The goal of the selection step is to report one single region per flow feature based on the results from the classification step. Each region from the region proposal step is assigned a probability by the CNN and classified as either background or flow feature. For discrete feature problems, many such regions describe the same feature. That is, multiple high probability windows are clustered around the correct location and have some overlap with each other. This is specially the case since the CNN is trained to positively classify partial features (typically as low as 50% overlap), and some of the cell volumes are very small. The goal is to report one single region per flow feature. This is achieved using greedy non-maximum suppression [10, 18], rejecting any region that overlaps another region with higher probability of being a feature, as illustrated in Fig. 6.

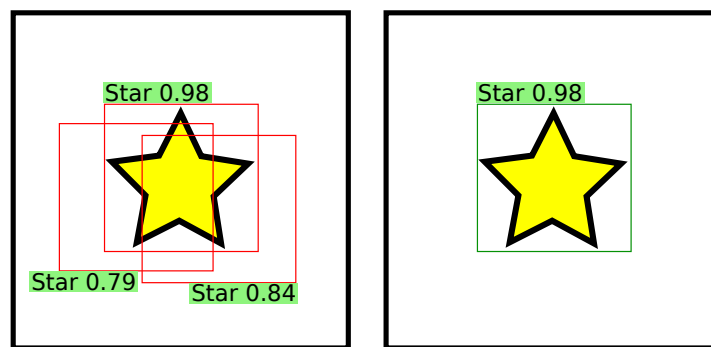


Figure 6: Example of how non-maximum suppression is used to select a single region for a given flow feature. In this example the region proposal and CNN evaluation results in a three regions above the classification threshold (left). Because the region with 84% probability overlaps with a region with higher probability (98%), this region is discarded. Similarly the region with 79% probability is also discarded. This leaves a single region for the given feature, which is the desired outcome.

The success of the method can be tested by using cases with known solutions, where the correct region has been labeled by a human. For *testing* cases, a successful identification is considered to be a selected region with IoU with a human labeled region above a

certain threshold (e.g. typically  $IoU \geq 0.5$  for object detection in images). The accuracy of the method can then be quantified by the percentage of regions that were correctly identified, as well as the percentage of false positives.

For continuous feature problems there are no discrete regions to be identified, but rather a continuum. For these cases selection was done by assigning a boolean value to each cell, with a *True* value for any cell that is within at least one of the regions classified by the CNN as being a feature. The selected region is then the union of all regions classified positively by the CNN. Since non-maximum suppression is not used for continuous feature problems, more aggressive choice of thresholds is needed to avoid selected regions that are much larger than the flow feature. In the context of the *feature extraction pipeline* presented in Post et al. [6] the presented method performs the selection step for both types of problems. It also performs the clustering step for the discrete feature problems but not for the continuous feature problems.

## 2.5 Implementation

The method was implemented in Python and runs in CPUs. We used the Lasagne [19] and Theano [20] libraries to create the CNN. The data creation task was parallelized with each training case evaluated independently. The CNN classification step was also parallelized with different batches of proposed regions sent to different CPUs. The training step was done in serial. As an example, Table 1 shows the computational cost and parallelization for the first case study. The largest costs are associated with the creation of training data (including the warping and interpolation) and the evaluation of the CNN. While some care was used to improve the cost, this was not the goal of this study and it can still be improved significantly. In image recognition there has been a push towards real-time identification, which is being achieved through algorithmic choices and GPU implementation. Some of the same techniques can be leveraged to speed-up our implementation.

Table 1: Summary of computational cost for Case study I. The evaluation values are for the convergent-divergent channel test case.

Task	No. CPUs	time [s]
Create training data (3 train cases)	3	1,069
Train (500 steps)	1	169
Evaluate regions with CNN	72	1,982

## 3 Results

Three case studies were investigated, using data from Reynolds-averaged Navier-Stokes (RANS) simulations. The first is a discrete feature problem: identifying the recirculation

region in 2D flows (Fig. 8, Fig. 9). The other two are continuous feature problems: identifying the boundary layer in 2D flows (Fig. 11), and a horseshoe vortex in a 3D flow (Fig. 13).

### 3.1 Case study I — Identifying 2D recirculation region

The first case study involved identifying regions of recirculation in 2D flows. This is a discrete feature problem, in which the CNN is trained using flow cases with the whole recirculation region labeled. The CNN was trained using three flows: periodic hills, wavy channel, and curved backwards-facing step. Each of these cases contained a single recirculation region, identified visually based on looping streamlines. The human-labeled recirculation region is shown for one of the training cases in Fig. 3. The methodology was then tested on two new flows: a convergent-divergent channel and flow over a NACA 0012 airfoil [21] at  $4^\circ$  angle of attack. These cases are summarized in Table 2 and shown in Fig. 7. The Reynolds number is based on the chord length and mean flow velocity for the airfoil and on the hill/step height and bulk mean velocity at the hill crest for all other cases. The RANS turbulence model used were the  $k-\omega$  SST for the airfoil and the Launder-Sharma  $k-\epsilon$  for all other cases.

Table 2: Summary of the four RANS cases used in Case study I and II.

Case	Reynolds Number	Mesh Size (rows $\times$ columns)	Use
Curved backwards-facing step	13,700	199 $\times$ 199	Training
Periodic hills	10,595	99 $\times$ 149	Training
Wavy channel	6,760	50 $\times$ 160	Training
Convergent-divergent channel	12,600	499 $\times$ 192	Testing
NACA 0012 airfoil	10,000	128 $\times$ 448	Testing

A CNN was trained using the three training examples. The CNN architecture consists of inputs size  $24 \times 24$ , ten feature maps in the convolutional layer with window size  $5 \times 5$  and max pooling with  $2 \times 2$  windows, and two dense layers of 10 ReLU and 2 softmax neurons consecutively. The CNN was trained for 500 training steps with a learning rate of 0.01 using mini-batches containing 5 recirculation cases, 5 difficult background cases, and 10 background cases.

The first test case was the convergent-divergent channel. This case was chosen as a test case since it is thought to contain a significantly different recirculation region, making it a difficult case to predict. The most noticeable difference is the long aspect ratio and short height of the recirculation region. The region proposal was done with 15 window sizes corresponding to aspect ratios of 1:1, 2:1, 1:2 and scale factor of 10, 20, 30, 40, 50 cells. A stride of 2 cells was used in each direction, resulting in 266,525 proposed regions. The Fluid R-CNN resulted in two regions selected as instances of recirculation, out of

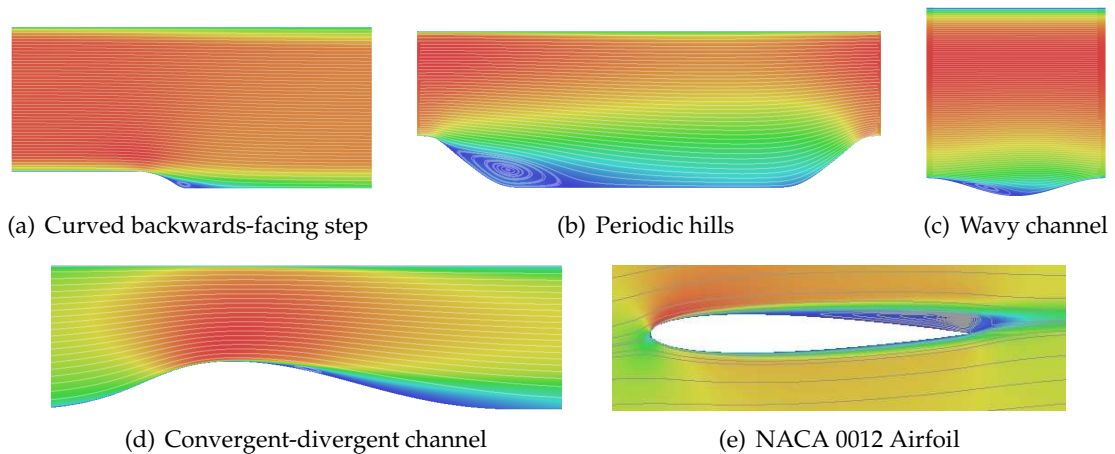


Figure 7: Simulation cases used in Case study I and II. The images show velocity magnitude as well as velocity streamlines. Blue and red denote the smallest and largest velocity magnitudes respectively.

2,242 evaluated positively by the CNN. One region was correctly selected, with a 98% probability of being recirculation, and an intersection over union of 68% with the human labeled region. The other region, a false positive, was assigned a 77% probability of being recirculation and has no intersection with any human labeled region. This false positive is likely due to the limited amount of training cases, which cannot provide enough training examples of all possible background regions. In the absence of large quantities of training data, a probability threshold can be manually tuned to a value higher than 50% to reduce these false positives. The results are summarized in Table 3 and shown in Fig. 8, with the two identified regions labeled. Fig. 8(b) also shows a close-up view of the streamlines in the two selected regions.

Table 3: Case study I results: list of selected regions with assigned probability of being a recirculation region and IoU with a correct, human-labeled, region.

Region	Probability	IoU with correct region
Convergent-Divergent Channel		
1	0.98	0.68
2	0.77	0.00
NACA 0012 Airfoil		
1	0.92	0.25
2	0.97	0.43

The second test cases is a NACA 0012 airfoil at  $4^\circ$  angle of attack. This case was added to provide a completely different flow geometry, an external flow. The mesh used in the airfoil case is from *NASA's Turbulence Modeling Resources* [21], and is significantly different than the meshes used in the training cases. The computational domain extends to 500

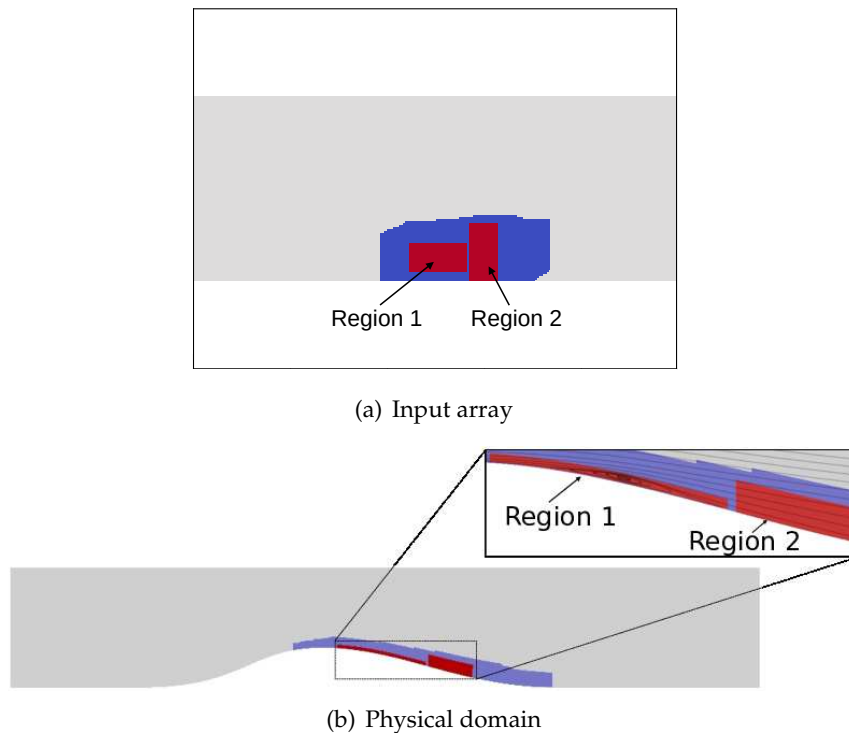


Figure 8: Case study I results: recirculation regions in the convergent-divergent channel flow. Blue denotes regions that the CNN classified as recirculation, and red denotes those regions selected as instances of recirculation.

chord lengths in any direction, the number of cells is small, and cells are concentrated towards the airfoil. This results in large ratios of largest to smallest cell volume, and large maximum aspect ratios. Since the mesh has a significant effect on the physical shape of regions and the warping to CNN inputs, this is a challenging case for a CNN trained with cases with very different meshes. The region proposal was done with 15 window sizes corresponding to aspect ratios of 2:2, 2:1, 1:2 and scale factor of 15, 20, 25, 30, 35 cells. A stride of 1 cell was used in each direction, resulting in 534,565 proposed regions. The Fluid R-CNN resulted in two regions selected as instances of recirculation, out of 2,731 evaluated positively by the CNN. One region was correctly selected, with a 92% probability of being recirculation, and an intersection over union of 25% with the human labeled region. The other region, a false positive, was assigned a 97% probability of being recirculation and an intersection over union of 43% with the human labeled region. While the IoU metric suggests both identifications were failure, it can be seen in Fig. 9 that the correct solution would be a single region roughly equal to the union of the two identified regions. These results are still promising considering that out of a domain of size roughly  $1,000 \times 1,000$  chord lengths the method was able to focus on the small region on the upper surface of the airfoil. Furthermore the method did initially identify single

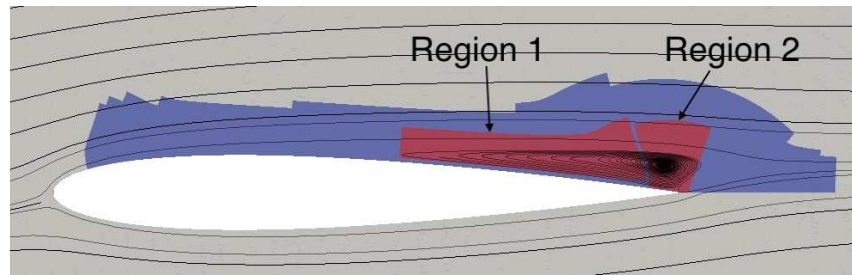


Figure 9: Case study I results: recirculation regions in the flow over an airfoil. Blue denotes regions that the CNN classified as recirculation, and red denotes those regions selected as instances of recirculation.

regions that more closely capture the whole recirculation but these were discarded during the non-maximum suppression step, indicating that the two separate regions were assigned higher probability than the single region. Again, this is likely due to the limited amount of training cases used to train the CNN. The results are summarized in Table 3 and shown in Fig. 9, with the two identified regions labeled.

### 3.2 Case study II — Identifying 2D boundary layer

For the second case study the boundary layer, a continuous feature, is identified in two different flows. The flows used are the periodic hills, and the convergent-divergent channel flows shown in Fig. 7. A CNN was trained using four section cuts from the periodic hills case, shown in Fig. 10. The boundary layer was identified visually based on wall-distance Reynolds number.

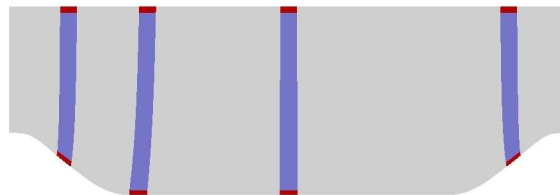


Figure 10: Section cuts (blue) and human-labeled boundary layer regions (red) used to train the boundary layer CNN for Case study II.

The CNN architecture was identical to that for Case study I. The CNN was trained for 500 training steps with a learning rate of 0.01 using mini-batches containing 5 boundary layer cases, no difficult background cases, and 15 background cases. All training windows were restricted to be the same width as the section cuts, namely 3 cells. The Fluid R-CNN was first tested on the entire periodic hill case, to identify the entire boundary layer after training with sectional cuts from the same case. The region proposal for the periodic hills case was done with 5 windows of width 3 and heights 10,15,20,25,30 cells with stride of 2 in both directions, resulting in 15,974 total regions. The results are shown in Fig. 11(a).

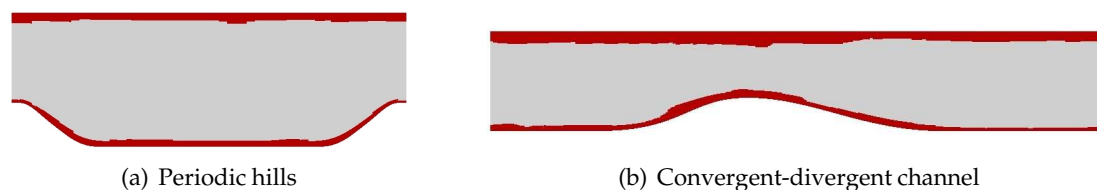


Figure 11: Case study II results: boundary layers (red/dark gray) in the periodic hills and convergent-divergent channel flows.

The Fluid R-CNN was then used on a new flow, the convergent-divergent channel, for which the CNN training saw no data from. The region proposal for the convergent-divergent channel case was done with 6 windows of width 3 and heights 10,20,30,40,50,60 cells with stride of 2 in both directions, resulting in 15,974 total regions. The results are shown in Fig. 11(b).

For both cases the algorithm was able to identify the entirety of the boundary layer. This was verified visually rather than quantitatively. One noticeable quirk of the results is that the boundary layer is significantly thicker than the human labeled examples used for training. This was expected since non-maximum suppression is not used for these cases, and the creation of training cases considers partial overlap regions (up to some IoU threshold) as examples of boundary layer. This behavior is inherent in the method used and cannot be eliminated, but some steps were taken to mitigate it. The IoU threshold was increased to 0.75 from the typical 0.5. In addition, since the boundary layer is a gradient with no clear edge, no difficult examples were used for background and its threshold was lowered to 0.1 from the typical 0.25. An alternative would be to use training examples with intermediate values of the probabilities for the different categories, rather than with examples labeled as 100% probability of belonging to one or the other.

### 3.3 Case study III — Identifying 3D horseshoe vortex

The third case study consists of identifying the horseshoe vortex in a 3D wing-body junction flow based on the experimental setup of Devenport et al. [22]. The problem is illustrated in Fig. 12. This is a continuous feature problem and the CNN was trained with section cuts of the domain. The Fluid R-CNN was then tested in the same flow in order to identify the entirety of the horseshoe vortex. The horseshoe vortex identification was done in only half the domain, but the results are mirrored for visualization. The RANS simulation for this case was done for half of the domain, using a symmetry plane, and a mesh size of  $149 \times 98 \times 49$  rows, columns, and layers respectively. The Reynolds number is about  $10^5$  based on airfoil thickness, and the turbulence model used was the  $k-\omega$  SST model.

A CNN was trained using four section cuts shown in Fig. 13(a). The horseshoe vortex was identified visually based on looping streamlines of the cross-flow components of velocity (no mean flow direction) at different cross-sections normal to the airfoil. The CNN

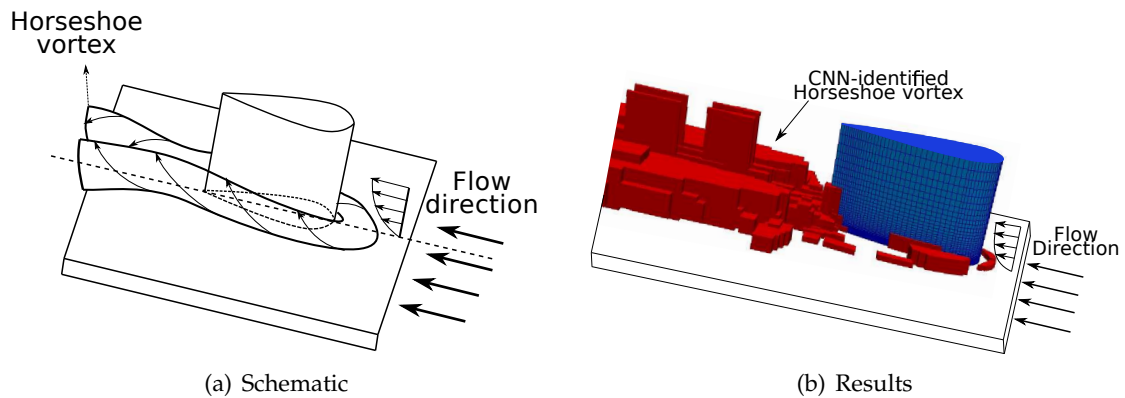


Figure 12: Schematic of a horseshoe vortex around the wing-body junction geometry used in Case study III (a), and results from the Fluid R-CNN method (b).

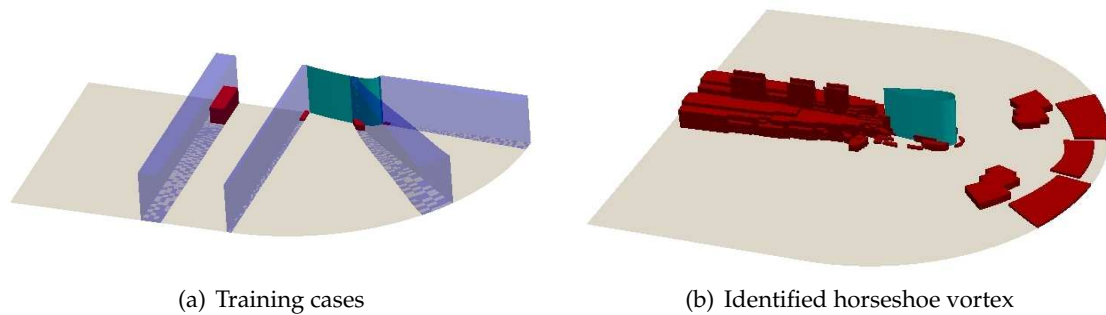


Figure 13: Case study III training cases (a) and results (b). The training cases consist of section cuts of the domain (blue) and human-labeled regions containing the horseshoe vortex (red). The results show the entire, mirrored, simulation domain including the wall (grey), airfoil (blue), and the identified vortex (red).

architecture consists of inputs size  $10 \times 10 \times 10$ , ten feature maps in the convolutional layer with window size  $4 \times 4 \times 4$  and max pooling with  $2 \times 2 \times 1$  windows, and two dense layers of 10 ReLU and 2 softmax neurons. Similar to boundary layer case, the training windows were restricted to be the same width as the section cuts. The mini-batches consisted of 5 horseshoe vortex cases, 5 difficult background cases, and 10 background cases with the IoU thresholds being the typical 0.5 and 0.25. The region proposal was done with 25 windows of width 3, height-to-depth ratios of 1:1, 1:2, 1:3, 1:4, 1:5 and scales 10, 20, 30, 40, 50 cells, with strides of (4, 1, 2) cells in the  $(x, y, z)$  directions, resulting in 181,728 total regions.

The results were evaluated qualitatively and are shown in Fig. 13(b). The Fluid R-CNN was able to identify most of the horseshoe vortex, doing particularly well downstream of the airfoil, but not as well around the airfoil where large portions of the vortex were not identified. The identified vortex in the wake also contains erroneous sections near the symmetry plain that extend far from the wall. The method also falsely identifies

a region of the wall near the inlet as horseshoe vortex. It is believed that these failures are due to the limited amount of training data, and the simplicity of the CNN architecture used.

## 4 Discussions

The goal of this study was to evaluate the potential of adapting a data-driven algorithm developed for image recognition to the problem of flow feature detection. The results are very encouraging, specially considering the limited amount of training data, the simplicity of the CNN architecture, and all the simplifications done to the overall R-CNN method. For instance, the recirculation CNN was trained using only three examples of recirculation. In image recognition it is typical to use hundreds to tens of thousand of images for any given category, and it is widely recognized that the best way to improve the performance of a CNN is by using more training data [13]. This and other important considerations need to be taken into account if this method will continue to be pursued.

### 4.1 Improving the Fluid R-CNN method

The Fluid R-CNN method can be improved at every stage using techniques already used in the image recognition counter-parts. The CNN classification can be improved by: (1) using more training examples and artificially augmenting the training data, (2) using deeper architecture and optimizing the architecture and training hyper-parameters, (3) using regularization techniques during training, such as dropout, to avoid over-fitting. For applications requiring identification of several classes of flow features the CNN could be used for local-feature extraction only, with classification done by class-specific support vector machines, allowing for greater specialization of these classifiers. For these cases a more sophisticated region proposal algorithm can be used, which would only pass the most likely regions to the classifiers. For cases with more than one instance of a feature of interest, an IoU threshold can be used on the non-maximum suppression at the selection step to allow for some amount of intersection between selected regions (see Fig. 2). As can be appreciated from this discussion, the methodology can become very complex very quickly. Although such complexities were not warranted for a first study into the adaptability of these methods to fluid flows, their incorporation should improve the performance significantly.

In this study the flows were restricted to flows with singly-connected domains, and were mapped to a rectangular domain. There are several ways of making this a general method. One possible approach would be to divide a multiply-connected domain into several singly-connected domains. The Fluid R-CNN method would first be used on each individually, and then regions along the boundaries which encompass two domains would need to be considered. Another approach we have tried with initial success is to completely forgo the domain mapping and search the physical domain directly, using

rectangular windows of fixed physical dimensions. The biggest challenge of this approach is in handling the boundaries, a problem shared with other fluid dynamics data post-processing techniques such as particle image velocimetry (PIV). Some of the same boundary-handling methods used in PIV could be used for the Fluid R-CNN method.

Another aspect of the formulation that requires more thought is the identification of continuous flow features, which has no analogue in image recognition. For instance addressing the issue with larger regions (e.g. thicker boundary layer) through either modifying the training data creation step or the selection step. Similarly, the clustering of the identified region into different instances of the flow feature was not considered in this study.

## 4.2 Application and limitations of the method

The method is shown to work reasonably well in the test cases presented and is expected to perform much better with more training data and better CNN architecture. However it must be pointed out that the computational cost of this method is much higher than existing identification methods based on calculating a field value and applying a threshold. For instance for vortex identification in time-dependent flows the  $Q$ -criterion or  $\lambda_2$ -criterion can be calculated and a threshold applied. This would be much faster and sufficient for many applications.

The advantage of the presented method comes in when there is no simple existing method for the feature in question, or when a higher level of granularity is desired in distinguishing between similar features. For instance the  $Q$ -criterion or  $\lambda_2$ -criterion methods are not applicable to identifying the recirculation regions in mean flows, as in the first case study. These two criteria are equivalent for planar incompressible flows and consist of a non-linear mapping from the three-dimensional velocity field to a scalar field. Due to the nonlinearities, the mapping applied to the mean velocity field is not equivalent to the time-average of the mapping applied to the instantaneous field. While the mapping can still be applied, the resulting scalar field will generally fail at identifying the recirculation region. For creating the training and testing examples the recirculation regions were determined manually by visualizing streamlines of the velocity field. The presented method would be a good choice for automatic detection of these features. The strength of this method is in being able to identify features solely from examples provided. The features themselves do not need to be well defined physically or mathematically as long as sufficient examples can be provided.

## 4.3 Extension to time-dependent cases

As discussed in the introduction, flow feature identification in time-dependent flow fields (e.g. coherent structures in turbulent flows) is an important application and motivation for the development of this method. While the current study focused on time-independent problems, the presented methodology can be used directly for identifying

flow features at individual time-steps in time-dependent flows. Time-dependent datasets have additional problems of interest, including event detection and feature tracking [6]. Feature tracking consist of determining if features at different times correspond to the same feature. Events in the time evolution of features include changing shape, splitting into two, dissipating, merging with another feature, and entering or leaving the domain. Two common approaches for feature tracking and event detection include extracting features from the spatial-temporal domain directly (e.g. treating the problem as four dimensional), or by extracting features at each separate time and solving the correspondence problem. The presented method should be useful in either of these approaches.

## 5 Conclusions

Feature identification is an important task in fluid dynamics applications. Existing methods are feature-specific and are based on physical understanding of the behavior of the flow at regions where the feature occurs. In this study convolutional neural networks, a machine learning technique developed for image recognition, were used to solve the problem of flow feature identification. These techniques work well because the two tasks, object detection in images and flow feature detection, are analogous. In particular, CNNs are well suited for flow feature identification because like objects in images, flow features can occur anywhere within the domain, and CNNs exploit this translation invariance. The novelty of the approach is that it is data-driven, performing the feature detection based on learning from training examples rather than on explicit interpretation of physical laws governing the flow. The method was proven to be successful by applying it to three different case studies: detecting recirculation regions and boundary layer in 2D RANS simulations, and horseshoe vortex in 3D RANS simulations. The results were surprisingly good for the limited amount of training data used and simplicity of the CNN architecture.

The main advantage of this data-driven method is that it is a general approach to feature extraction rather than being feature-specific, with the ability to detect new features for which a physics based detection method does not exist. Being a data-driven method, it potentially has the ability to distinguish between very similar features, provided enough training data. There are also some challenges with this data-driven method. The method relies on a large amount of human-labeled training data, which can be difficult to obtain. The method is also more computationally intensive than some of the current techniques that rely on calculation of a single quantity at each point. Because of this, the method is more useful for flow features which have no existing method of calculating a field value used for feature identification. For instance, while vortex identification methods, such as the  $Q$ -criterion or  $\lambda_2$ -criterion, exist for identifying these features in time-dependent flows, such methods cannot be directly applied for recirculation regions in the mean flow. The method could also be useful to differentiate between different type of vortex structures, which could not be done with existing methods.

In this study we have demonstrated that data-driven methods can provide a general approach to flow feature extraction. Future work will focus on improving the performance by incorporating the changes discussed in Section 4.1 and using the method for identifying flow features in time-dependent flows.

## Acknowledgments

The authors thank Dr. Todd Lowe at Virginia Tech for his valuable input throughout the project, Dr. Lian Duan at Missouri S&T for his support on developing the background material, and Yang Zeng for his help in creating some of the images. This work was in part possible thanks to the Kevin T. Crofton Graduate Fellowship.

## Appendix

### A Input parameters

This appendix summarizes the ten input parameters used from Wang et al. [15] and Ling et al. [16]. The definition of the invariants is shown in Table 5. These inputs are non-dimensional and Galilean invariant. Each input  $q$  is obtained by

$$q = \frac{\hat{q}}{(|\hat{q}| + |q^*|)}, \quad (\text{A.1})$$

Table 4: Nomenclature for input definition.

Symbol	Definition
$U_i$	Mean velocity
$k$	Turbulent kinetic energy
$u'_i$	Fluctuation velocity
$\rho$	Fluid density
$\varepsilon$	Turbulence dissipation rate
$\mathbf{S}$	Strain rate tensor
$\mathbf{\Omega}$	Rotation rate tensor
$\nu$	Fluid viscosity
$d$	Wall distance
$\mathbf{\Gamma}$	Unit tangential velocity vector
$L_c$	Characteristic mean flow length scale
$P$	Fluid pressure
$x_i$	Position
$t$	Time

Table 5: Non-dimensional flow features used as input in the classification.

Input ( $q$ )	Raw input ( $\hat{q}$ )	Normalization factor ( $q^*$ )
Ratio of excess rotation rate to strain rate ( $Q$ -criterion)	$\frac{1}{2}(\ \boldsymbol{\Omega}\ ^2 - \ \mathbf{S}\ ^2)$	$\ \mathbf{S}\ ^2$
Turbulence intensity	$k$	$\frac{1}{2}U_i U_i$
Wall-distance based Reynolds number	$\min\left(\frac{\sqrt{k}d}{50\nu}, 2\right)$	—
Pressure gradient along streamline	$U_k \frac{\partial P}{\partial x_k}$	$\sqrt{\frac{\partial P}{\partial x_j} \frac{\partial P}{\partial x_j} U_i U_i}$
Ratio of turbulent time scale to mean strain time scale	$\frac{k}{\varepsilon}$	$\frac{1}{\ \mathbf{S}\ }$
Ratio of pressure normal stresses to shear stresses	$\sqrt{\frac{\partial P}{\partial x_i} \frac{\partial P}{\partial x_i}}$	$\frac{1}{2\rho} \frac{\partial U_k^2}{\partial x_k}$
Non-orthogonality between velocity and its gradient	$\left U_i U_j \frac{\partial U_i}{\partial x_j}\right $	$\sqrt{U_l U_l U_i \frac{\partial U_i}{\partial x_j} U_k \frac{\partial U_k}{\partial x_j}}$
Ratio of convection to production of TKE	$U_i \frac{dk}{dx_i}$	$ \overline{u'_j u'_k} S_{jk} $
Ratio of total to normal Reynolds stresses	$\ \overline{u'_i u'_j}\ $	$k$
Streamline curvature	$\left \frac{D\boldsymbol{\Gamma}}{ \mathbf{U} Df}\right $	$\frac{1}{L_c}$

where  $\hat{q}$  and  $q^*$  are the *raw* input and normalization factor respectively. The exception is wall-distance based Reynolds number which does not require a normalization parameter and is given by  $q = \hat{q}$ . The definition of non-orthogonality of velocity and its gradient comes from Gorle et al. [23]. The nomenclature for the variables used in Table 5 is given in Table 4. Repeated indices imply summation,  $D$  denotes the total derivative,  $\|\cdot\|$  the matrix norm, and  $|\cdot|$  the vector norm.

## References

- [1] A. K. M. Fazle Hussain. Coherent structures and turbulence. *J. Fluid Mech.*, 173(-1):303, December 1986.
- [2] S. K. Robinson. Coherent motions in the turbulent boundary layer. *Annu. Rev. Fluid Mech.*, 23(1):601–639, 1991.
- [3] Dennis M. Bushnell. Shock wave drag reduction. *Annu. Rev. Fluid Mech.*, 36(1):81–96, 2004.
- [4] John Van Rosendale. Floating shock fitting via Lagrangian adaptive meshes. In *12th Computational Fluid Dynamics Conference*. American Institute of Aeronautics and Astronautics, June 1995.
- [5] S. J. Kamkar, A. M. Wissink, V. Sankaran, and A. Jameson. Feature-driven Cartesian adaptive mesh refinement for vortex-dominated flows. *J. Comput. Phys.*, 230(16):6271–6298, July 2011.
- [6] Frits H. Post, Benjamin Vrolijk, Helwig Hauser, Robert S. Laramee, and Helmut Doleisch. The state of the art in flow visualisation: Feature extraction and tracking. In *Computer Graphics Forum*, volume 22, pages 775–792. Wiley Online Library, 2003.
- [7] Jochen Fröhlich, Christopher P. Mellen, Wolfgang Rodi, Lionel Temmerman, and Michael A. Leschziner. Highly resolved large-eddy simulation of separated flow in a channel with streamwise periodic constrictions. *J. Fluid Mech.*, 526:19–66, March 2005.
- [8] M. Breuer, N. Peller, Ch. Rapp, and M. Manhart. Flow over periodic hills: Numerical and experimental study in a wide range of reynolds numbers. *Comput. Fluids*, 38(2):433–457, 2009.
- [9] Jiequn Han, Linfeng Zhang, Roberto Car, et al. Deep Potential: A general representation of a many-body potential energy surface. *Commun. Comput. Phys.*, 23:629–639, 2018.
- [10] Ross Girshick, Jeff Donahue, Trevor Darrell, and Jitendra Malik. Rich feature hierarchies for accurate object detection and semantic segmentation. In *Proceedings of the IEEE conference on computer vision and pattern recognition*, pages 580–587, 2014.
- [11] Shaoqing Ren, Kaiming He, Ross Girshick, and Jian Sun. Faster R-CNN: Towards real-time object detection with region proposal networks. In *Advances in neural information processing systems*, pages 91–99, 2015.
- [12] Yann LeCun, Leon Bottou, Yoshua Bengio, and Patrick Haffner. Gradient-based learning applied to document recognition. *Proc. IEEE*, 86:2278–2324, November 1998.
- [13] Patrice Simard, Dave Steinkraus, and John Platt. Best practices for convolutional neural networks applied to visual document analysis. In *Proceedings of the seventh international conference on document analysis and recognition*, 2003.
- [14] Michael A. Nielsen. *Neural Networks and Deep Learning*. 2015.
- [15] Jian-Xun Wang, Jin-Long Wu, and Heng Xiao. Physics-informed machine learning approach for reconstructing Reynolds stress modeling discrepancies based on DNS data. *Phys. Rev. Fluids*, 2(3), March 2017.
- [16] J. Ling and J. Templeton. Evaluation of machine learning algorithms for prediction of regions of high Reynolds averaged Navier Stokes uncertainty. *Phys. Fluids*, 27(8):085103, March 2015.
- [17] David E Rumelhart, Geoffrey E Hinton, and Ronald J Williams. Learning representations by back-propagating errors. *Nature*, 323(6088):533, 1986.
- [18] Pedro F Felzenszwalb, Ross B Girshick, David McAllester, and Deva Ramanan. Object detection with discriminatively trained part-based models. *IEEE Trans. Pattern Anal. Mach. Intell.*, 32(9):1627–1645, 2010.
- [19] Sander Dieleman, Jan Schlter, Colin Raffel, Eben Olson, Sren Kaae Snderby, Daniel Nouri, et al. Lasagne: First release., August 2015.

- [20] Theano Development Team. Theano: A Python framework for fast computation of mathematical expressions. *arXiv e-prints*, abs/1605.02688, May 2016.
- [21] NASA Langley Research Center turbulence modeling resource. <https://turbmodels.larc.nasa.gov/index.html>.
- [22] William J. Devenport and Roger L. Simpson. Time-dependent and time-averaged turbulence structure near the nose of a wing-body junction. *J. Fluid Mech.*, 210:2355, 1990.
- [23] Catherine Gorle, Michael Emory, and Gianluca Iaccarino. RANS modeling of turbulent mixing for a jet in supersonic cross flow: Model evaluation and uncertainty quantification. In *ICHMT DIGITAL LIBRARY ONLINE*. Begel House Inc., 2012.